Transformation textures in post-perovskite: Understanding mantle flow in the D″ layer of the Earth

N. P. Walte,[1] F. Heidelbach,[1] N. Miyajima,[1] D. J. Frost,[1] D. C. Rubie,[1] and D. P. Dobson[2]

Received 3 December 2008; revised 9 January 2009; accepted 16 January 2009; published 18 February 2009.

[1] Deformation and texture formation in (Mg, Fe)SiO_3 post perovskite (ppv) is a potential explanation for the strong seismic anisotropy that is found in the D″ layer of the Earth. However, different experimental approaches have resulted in different lattice preferred orientations (LPO) in deformed ppv that have led to ambiguity in the interpretation of deformation in the lowermost mantle. Here, we show that deformation of the analogue substance $CaIrO_3$ during a phase transformation from perovskite to ppv leads to a transformation texture that differs from the $CaIrO_3$ ppv deformation texture but resembles the results from ppv deformation experiments in diamond anvil cells. Assuming material spreading parallel to the core-mantle boundary, our results predict a widespread shear wave splitting with fast horizontal S-waves, which is compatible with seismic studies. Downwelling material that undergoes a phase transformation may develop a transformation texture that would locally result in vertically polarized fast S-waves. **Citation:** Walte, N. P., F. Heidelbach, N. Miyajima, D. J. Frost, D. C. Rubie, and D. P. Dobson (2009), Transformation textures in post-perovskite: Understanding mantle flow in the D″ layer of the Earth, *Geophys. Res. Lett.*, *36*, L04302, doi:10.1029/2008GL036840.

1. Introduction

[2] The transition from the Earth's lower mantle into the 200–300 km thick D″ layer near the core-mantle boundary is characterized by a switch from a seismically near-isotropic region to a layer of great seismic complexity. Seismic investigations of the D″ layer have revealed large low-shear-velocity provinces (LLSVP) [*Trampert et al.*, 2004], ultralow-velocity zones (ULVZ) [*Garnero et al.*, 1998], and shear-wave splitting. Shear waves that graze the D″ layer at a low angle split into horizontally polarized waves with a usually higher velocity and vertically polarized S-waves with a slightly lower velocity ($V_{SH} > V_{SV}$) [*Garnero and Lay*, 2003; *Panning and Romanowicz*, 2004; *van der Hilst et al.*, 2007], although some parts of the D″ layer appear to be more isotropic [*Garnero et al.*, 2004b]. With the discovery of the post-perovskite phase (ppv) that occurs at the pressure and temperature conditions of the D″ layer [*Murakami et al.*, 2004] a new candidate became available to explain the occurrence and seismic complexity of the D″ layer. It was suggested that a deformation induced lattice preferred orientation (LPO) could be the cause for the shear wave splitting [*Murakami et al.*, 2004]. If a strong link between seismic observations and ppv deformation behaviour could be established, more detailed investigations of mantle flow patterns would become possible in the lowermost Earth's mantle.

[3] The seismic properties of deformed polycrystalline aggregates can be derived from the LPO of experimentally-deformed samples [*Mainprice*, 1990]. However, since the high pressure of the ppv stability field (>125 GPa) inhibits conventional deformation experiments, two alternative experimental approaches have been followed to investigate the LPO of ppv: (i) Deformation of $MgGeO_3$ and $MgSiO_3$ ppv by axial shortening in a diamond anvil cell apparatus (DAC) [*Merkel et al.*, 2006, 2007]. These studies suggest the dominance of {100} or {110} glide planes in ppv. Modeling of seismic anisotropy from the DAC experiments predicted a shear wave splitting with a mainly vertical polarization of the fast S-waves for the D″ layer [*Merkel et al.*, 2007]. (ii) Controlled deformation of the isostructural ppv analogue substance $CaIrO_3$ [*Miyagi et al.*, 2008; *Walte et al.*, 2007; *Yamazaki et al.*, 2006]. $CaIrO_3$ ppv is stable at ambient conditions, and forms a pv structure at higher temperatures [*Hirose and Fujita*, 2005]. The analogue experiments resulted in a dominant [100]{010} glide system [*Walte et al.*, 2007; *Yamazaki et al.*, 2006]. Modeling of seismic anisotropy based on the $CaIrO_3$ textures predicted an S-wave splitting with a polarization of the fast S-waves parallel to the shear plane, which is consistent with measured S-wave splitting in the D″ layer [*Walte et al.*, 2007; *Yamazaki et al.*, 2006].

[4] The reason for the diametrically opposite LPOs obtained using the two experimental approaches is currently unclear. While some authors debate the validity of $CaIrO_3$ as a good mechanical analogue for $MgSiO_3$ ppv [e.g., *Miyagi et al.*, 2008], other authors point out that most of the deformation in the DAC experiments occurs during the phase transformation to $MgSiO_3$ ppv, which may produce a transformation texture [*Walte et al.*, 2007]. In this study we performed $CaIrO_3$ deformation experiments during the pv-ppv phase transformation to investigate whether the transition has an influence on the textural development.

2. Experimental Procedure

[5] The experiments were performed with a deformation-DIA multianvil apparatus (d-DIA) [*Wang et al.*, 2003]. Details of the experimental procedure can be found in Walte et al. [*Walte et al.*, 2007]. For the pv-ppv transformation experiments the samples were brought into the $CaIrO_3$ pv stability field at 1 GPa and 1450°C and annealed for ca. 2 hours (Figure 1). After the start of axial shortening the temperature was decreased to the ppv stability field and deformation was continued for times ranging from 5

[1]Bayerisches Geoinstitut, Universität Bayreuth, Bayreuth, Germany.
[2]Department of Earth Sciences, University College London, London, UK.

0094-8276/09/2008GL036840

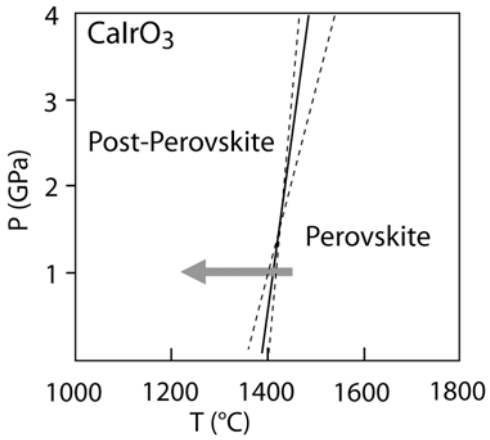

Figure 1. $CaIrO_3$ phase diagram redrawn after *Kojitani et al.* [2007]. For the transformation experiments the samples were annealed in the pv field. During deformation the temperature was decreased to 1200–1300°C into the ppv field (arrow).

minutes to 12 hours before rapid quenching (Table 1). The results of these transformation experiments are compared with results from two control experiments in which $CaIrO_3$ was deformed from the beginning in the ppv stability field.

[6] Sample imaging was performed by SEM orientation contrast analysis (OC); texture analysis was performed with SEM electron backscatter diffraction analysis (EBSD) with a LEO Gemini 1530 at 20 or 30 kV accelerating voltage and 4 nA beam current. $CaIrO_3$ pv is orthorhombic (pseudo-cubic) both at room and experimental conditions; with the EBSD technique it was indexed as cubic because the orthorhombic distortion was not distinguishable.

3. Results

[7] The samples from the transformation experiments consist of a mixture of relict pv and newly formed ppv grains. Newly grown ppv often forms fine-grained rims that are in contact with large relict pv grains; further pv-ppv reaction progress produces coarser-grained polycrystalline ppv regions that surround relict pv crystals. Often the ppv rims display only minor internal deformation features, while larger ppv grains frequently show irregular grain boundaries and abundant subgrains, which are indications for intra-crystalline deformation. Few ppv grains can be found inside larger pv grains, which suggests that the main nucleation sites are the pv grain boundaries.

[8] EBSD analysis of the recovered samples reveals different LPOs between the transformation experiments and the deformation experiments of the control group (Figure 2a). The transformation experiments resulted in a LPO characterized by an alignment of the poles to the {100} and {110} planes approximately parallel to the compression axis. The control experiments are characterized by an alignment of the {010} poles parallel to the compression axis. In some transformation experiments both textures can be found in a single sample: small, barely deformed ppv grains show a {100} and {110} alignment parallel to the compression axis, while the coarser, more-deformed, ppv grains are characterized by a rough alignment of {010} poles parallel to the compression axis (Figure 3). Hence, ppv grains initially grow with a {100} or {110} pole orientation parallel to the compression axis, whereas progressive deformation of the ppv grains after their formation rotates the crystal lattices and forms a {010} pole maximum. EBSD measurements of the relict pv grains in the transformation samples do not reveal a discernible LPO. This is consistent with previous LPO measurements of deformed $CaIrO_3$ pv [*Walte et al.*, 2007].

[9] The EBSD data from Figure 2a was combined with the theoretically-derived single crystal elastic tensor of *Stackhouse et al.* [2005] to model the seismic properties of the polycrystalline aggregates using the method and software of *Mainprice* [1990] (Figure 2b). The calculated P-wave anisotropy for the transformation texture is 1.6% with the maximum velocity parallel to the shortening direction and the minimum velocity in the shear plane. The sample displays a shear wave splitting with a maximum of 2.8% with a near-vertical polarization of the fast S-waves. Seismic modeling of the constant temperature experiment results in a P-wave anisotropy of 3.2% with the maximum velocity in the shear plane and a shear wave splitting of 3% with a generally horizontal polarization of the fast S-waves (Figure 2b). Using the elastic tensor of *Wentzcovitch et al.* [2006] for seismic modeling results in similar but slightly smaller anisotropy.

4. Discussion and Conclusion

[10] Our results indicate that $CaIrO_3$ ppv can develop two different LPOs during deformation: (i) Newly grown ppv

Table 1. Summary of the D-DIA Experiments[a]

Number	Temperature (°C)	Pressure (GPa)	Strain Rate (s^{-1})	Bulk Shortening	Time in PPV Field	LPO
			PV-PPV Transformation Experiments			
DD 310	1300	1	$4*10^{-4}$	20%	5 min	weak T-LPO
DD 309	1200	1	$5*10^{-4}$	40%	11 min	mixed (Figure 3)
DD 273	1300	1	$1.7*10^{-4}$	27%	24 min	T-LPO
DD 266	1200	1	$7.4*10^{-5}$	23%	1 h	T-LPO
DD 253	1200	1	$3.5*10^{-5}$	47%	3.5 h	T-LPO
DD 231	1400	1	$2.5*10^{-5}$	46%	5 h	Oblique T-LPO
DD 257	1000	1	$2.7*10^{-5}$	53%	7.25 h	Oblique D-LPO
DD 326	1300	1	10^{-5}	40%	11.5 h	D-LPO
			PPV Deformation Experiments			
DD 88	1200	3	$3*10^{-5}$	30%	170 min	D-LPO
DD 96	1400	2	10^{-4}	70%	1 h	D-LPO (Figure 3)

[a]T-LPO, transformation texture, poles of {100}/{110} parallel to compression axis. D-LPO, deformation texture, poles of {010} parallel to compression axis.

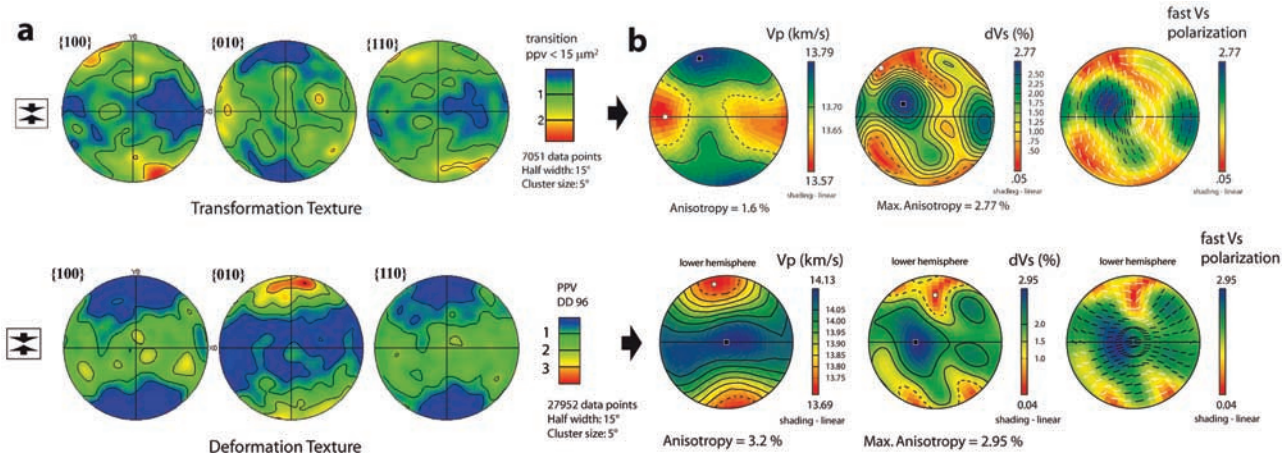

Figure 2. Lower hemisphere projections of (a) deformed ppv samples and (b) corresponding calculations of seismic velocities. LPO of ppv grains smaller than 15 mm^2 combined of two short transformation experiments (DD 309, DD 310) (Figure 2a (top)). The grains display a transformation texture with poles of {100}/{110} aligned in the compression axis. (bottom) Post perovskite deformation texture (DD 96) with poles of {010} aligned in the compression axis. Calculated seismic p- and s-wave velocities using the elastic tensor of *Stackhouse et al.* [2005] at 3000 K and 136 Gpa (Figure 2b). Note the largely vertical polarization of the fast S-waves for the transformation texture ($V_{SH} < V_{SV}$) (Figure 2b (top)) and the horizontal polarization for the deformation texture ($V_{SH} > V_{SV}$) (Figure 2b (bottom)).

acquires a transformation texture, with the poles of the {100} and {110} planes aligned in the compression axis when the pv-ppv boundary is crossed. (ii) ppv that is deformed in the ppv stability field acquires a deformation texture characterized by the [100]{010} glide system. Intermediate textures are formed when samples with an initial transformation texture are deformed in the ppv field. Hence, the deformation texture can either be found in samples that were deformed entirely in the ppv stability field or in ppv grains that were strongly deformed after their growth.

[11] It is currently unclear how transformation textures form. Texture inheritance from pv can be excluded since the relict pv is untextured. One possibility would be an oriented nucleation and growth of ppv in the stress field as was suggested for the olivine-wadsleyite transformation [*Dupas-Bruzek et al.*, 1998]; alternatively ppv could be formed by a martensitic-like reaction similar to the olivine-ringwoodite transformation [*Kerschhofer et al.*, 1996]. Based on numerical simulations, *Oganov et al.* [2005] suggest that stacking faults on {010} of pv as well as on {110} of ppv provide a mechanism for the pv-ppv phase transformation. However, we could not observe a preferred orientation relationship between {110} of ppv and {010} of pv in the partly transformed samples by EBSD mapping. Since no systematic orientation relationship of ppv with relict pv grains was detected and nucleation of ppv is concentrated at grain

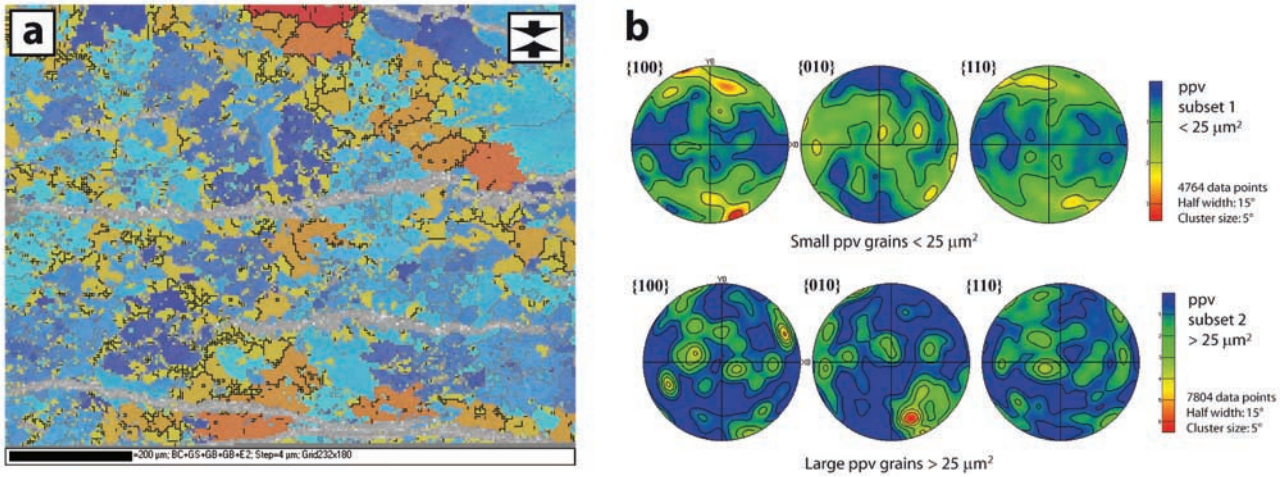

Figure 3. Two texture types in a transformation experiment (DD 309). (a) EBSD map showing relict perovskite grains (blue) and new ppv grains (orange). Grey horizontal features are quench cracks. Larger ppv grains are situated in monomineralic regions, while the centre is dominated by finer-grained ppv crystals. (b) Pole figure s of the (top) fine-grained subset display a transformation texture; the older, (bottom) coarse-grained subset displays an oblique deformation texture.

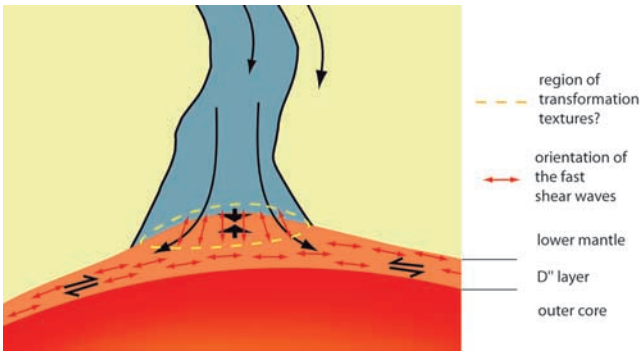

Figure 4. Sketch of the core-mantle region of the Earth. Material entering the D″ region undergoes a pv-ppv phase transition and simultaneous bulk dip-parallel shortening. A transformation texture may locally cause vertically polarized fast S-waves. Core-mantle parallel shearing produces a deformation texture with dominantly horizontally polarized fast S-waves.

boundaries, oriented nucleation and growth appears to be the most likely transformation mechanism.

[12] The LPOs and calculated seismic anisotropies of our transformation experiments are almost identical to the results of the DAC experiments of *Merkel et al.* [2006, 2007]. We therefore conclude that these experiments recorded the transformation textures of $MgGeO_3$ and $MgSiO_3$ and that [100]{010} is the dominant slip system of ppv, which confirms recent numerical modeling of both $MgSiO_3$ and $CaIrO_3$ ppv [*Carrez et al.*, 2007; *Metsue et al.*, 2009]. It is not entirely clear why no intermediate textures were found in the DAC experiments. Since deformation is hindered as the gasket gets thinner, the strain after ppv formation was perhaps not sufficient for a detectible texture rotation.

[13] Using a simplified model of material flow our results can be applied to the lowermost mantle as follows (Figure 4). Downwelling material is shortened in the direction of slab-dip as it enters D″, which may result in a transformation texture leading to fast vertically polarized S-waves. As the material sinks deeper and spreads laterally, shearing parallel to the core-mantle boundary forms a deformation texture, resulting in fast horizontally polarized S-waves. This model is compatible with a general S-wave splitting with $V_{SH} > V_{SV}$ that is observed in many parts of the D″ layer [*Kendall*, 2000]. Transformation textures might most likely be observed in regions of D″, which have seen a long history of downwelling. Possible examples are regions beneath the Cocos plate and Northern Siberia for which studies have resulted in inclined angles of the fast S-waves [*Garnero et al.*, 2004a; *Wookey and Kendall*, 2008]. This might be compatible with a transformation texture component. Indications for an increase of seismic anisotropy from top to bottom in D″ [*Garnero and McNamara*, 2008] could also be the result of texture interference or may reflect a strain rate increase with depth. Alternative suggestions for the seismic anisotropy of the D″ layer such as a LPO in (Mg, Fe)O [*Karki et al.*, 1999] cannot explain why seismic anisotropy is not observed in the deeper parts of the lower mantle. However, the contribution of (Mg, Fe)O for deformation and texture development in the D″ layer needs to be investigated further.

[14] For evaluating the possible importance of transformation textures in the Earth, seismic anisotropy in areas of the D″ layer with a long subduction history have to be compared in detail with areas not affected by subduction. A better understanding of the pv-ppv transformation mechanism and the interplay between transformation and deformation in ppv will help to understand the relation between texture, seismic anisotropy, and flow directions in the lowermost mantle.

[15] **Acknowledgments.** E. Garnero and an anonymous reviewer provided constructive reviews. N.W. acknowledges support from the European Science Foundation under the EUROCORES program EuroMinSci, contract ERAS-CT-2003-980409 of the European Commission, DG Research, FP6.

References

Carrez, P., D. Ferre, and P. Cordier (2007), Peierls-Nabarro model for dislocations in $MgSiO_3$ post-perovskite calculated at 120 GPa from first principles, *Philos. Mag.*, *87*(22), 3229–3247.

Dupas-Bruzek, C., T. G. Sharp, D. C. Rubie, and W. B. Durham (1998), Mechanisms of transformation and deformation in $Mg_{1.8}Fe_{0.2}SiO_4$ olivine and wadsleyite under non-hydrostatic stress, *Phys. Earth Planet. Inter.*, *108*(1), 33–48.

Garnero, E. J., and T. Lay (2003), D″ shear velocity heterogeneity, anisotropy and discontinuity structure beneath the Caribbean and Central America, *Phys. Earth Planet. Inter.*, *140*(1–3), 219–242.

Garnero, E. J., and A. K. McNamara (2008), Structure and dynamics of Earth's lower mantle, *Science*, *320*(5876), 626–628.

Garnero, E. J., J. Revenaugh, T. Lay, and L. H. Kellog (1998), Ultralow velocity zone at the core-mantle boundary, in *The Core-Mantle Boundary Region*, *Geodyn. Ser.*, vol. 28, edited by M. Gurnis et al., pp. 319–334, AGU, Washington, D.C.

Garnero, E. J., V. Maupin, T. Lay, and M. J. Fouch (2004a), Variable azimuthal anisotropy in Earth's lowermost mantle, *Science*, *306*(5694), 259–261.

Garnero, E. J., M. M. Moore, T. Lay, and M. J. Fouch (2004b), Isotropy or weak vertical transverse isotropy in D″ beneath the Atlantic Ocean, *J. Geophys. Res.*, *109*, B08308, doi:10.1029/2004JB003004.

Hirose, K., and Y. Fujita (2005), Clapeyron slope of the post-perovskite phase transition in $CaIrO_3$, *Geophys. Res. Lett.*, *32*, L13313, doi:10.1029/2005GL023219.

Karki, B. B., R. M. Wentzcovitch, S. de Gironcoli, and S. Baroni (1999), First-principles determination of elastic anisotropy and wave velocities of MgO at lower mantle conditions, *Science*, *286*(5445), 1705–1707.

Kendall, J. M. (2000), Seismic anisotropy in the boundary layers of the mantle, in *Earth's Deep Interior: Mineral Physics and Tomography From the Atomic to the Global Scale*, *Geophys. Monogr. Ser.*, vol. 117, edited by S. Karato et al., pp. 133–159, AGU, Washington, D.C.

Kerschhofer, L., T. G. Sharp, and D. C. Rubie (1996), Intracrystalline transformation of olivine to wadsleyite and ringwoodite under subduction zone conditions, *Science*, *274*(5284), 79–81.

Kojitani, H., A. Furukawa, and M. Akaogi (2007), Thermochemistry and high-pressure equilibria of the post-perovskite phase transition in $CaIrO_3$, *Am. Mineral.*, *92*(1), 229–232.

Mainprice, D. (1990), A FORTRAN program to calculate seismic anisotropy from the lattice preferred orientation of minerals, *Comput. Geosci.*, *16*(3), 385–393.

Merkel, S., A. Kubo, L. Miyagi, S. Speziale, T. S. Duffy, H. K. Mao, and H. R. Wenk (2006), Plastic deformation of $MgGeO_3$ post-perovskite at lower mantle pressures, *Science*, *311*(5761), 644–646.

Merkel, S., A. K. McNamara, A. Kubo, S. Speziale, L. Miyagi, Y. Meng, T. S. Duffy, and H. R. Wenk (2007), Deformation of (Mg, Fe)SiO_3 post-perovskite and D″ anisotropy, *Science*, *316*(5832), 1729–1732.

Metsue, A., P. Carrez, D. Mainprice, and P. Cordier (2009), Numerical modelling of dislocations and deformation mechanisms in $CaIrO_3$ and $MgGeO_3$ post-perovskites—Comparison with $MgSiO_3$ post-perovskite, *Phys. Earth Planet. Inter.*, in press.

Miyagi, L., N. Nishlyama, Y. B. Wang, A. Kubo, D. V. West, R. J. Cava, T. S. Duffy, and H. R. Wenk (2008), Deformation and texture development in $CaIrO_3$ post-perovskite phase up to 6 GPa and 1300 K, *Earth Planet. Sci. Lett.*, *268*(3–4), 515–525.

Murakami, M., K. Hirose, K. Kawamura, N. Sata, and Y. Ohishi (2004), Post-perovskite phase transition in $MgSiO_3$, *Science*, *304*(5672), 855–858.

Oganov, A. R., R. Martonak, A. Laio, P. Raiteri, and M. Parrinello (2005), Anisotropy of Earth's D″ layer and stacking faults in the $MgSiO_3$ post-perovskite phase, *Nature*, *438*(7071), 1142–1144.

Panning, M., and B. Romanowicz (2004), Inferences on flow at the base of Earth's mantle based on seismic anisotropy, *Science*, *303*(5656), 351–353.

Stackhouse, S., J. P. Brodholt, and G. D. Price (2005), High temperature elastic anisotropy of the perovskite and post-perovskite polymorphs of Al_2O_3, *Geophys. Res. Lett.*, *32*, L13305, doi:10.1029/2005GL023163.

Trampert, J., F. Deschamps, J. Resovsky, and D. Yuen (2004), Probabilistic tomography maps chemical heterogeneities throughout the lower mantle, *Science*, *306*(5697), 853–856.

van der Hilst, R. D., M. V. de Hoop, P. Wang, S. H. Shim, P. Ma, and L. Tenorio (2007), Seismostratigraphy and thermal structure of Earth's core-mantle boundary region, *Science*, *315*(5820), 1813–1817.

Walte, N., F. Heidelbach, N. Miyajima, and D. Frost (2007), Texture development and TEM analysis of deformed $CaIrO_3$: Implications for the D″ layer at the core-mantle boundary, *Geophys. Res. Lett.*, *34*, L08306, doi:10.1029/2007GL029407.

Wang, Y. B., W. B. Durham, I. C. Getting, and D. J. Weidner (2003), The deformation-DIA: A new apparatus for high temperature triaxial deformation to pressures up to 15 GPa, *Rev. Sci. Instrum.*, *74*(6), 3002–3011.

Wentzcovitch, R. M., T. Tsuchiya, and J. Tsuchiya (2006), $MgSiO_3$ post-perovskite at D″ conditions, *Proc. Natl. Acad. Sci. U. S. A.*, *103*(3), 543–546.

Wookey, J., and J. M. Kendall (2008), Constraints on lowermost mantle mineralogy and fabric beneath Siberia from seismic anisotropy, *Earth Planet. Sci. Lett.*, *275*(1–2), 32–42.

Yamazaki, D., T. Yoshino, H. Ohfuji, J. I. Ando, and A. Yoneda (2006), Origin of seismic anisotropy in the D″ layer inferred from shear deformation experiments on post-perovskite phase, *Earth Planet. Sci. Lett.*, *252*(3–4), 372–378.

D. P. Dobson, Department of Earth Sciences, University College London, Gower Street, London WC1E 6BT, UK.

D. J. Frost, F. Heidelbach, N. Miyajima, D. C. Rubie, and N. P. Walte, Bayerisches Geoinstitut, Universität Bayreuth, D-95440 Bayreuth, Germany. (nico.walte@uni-bayreuth.de)